

Heavy carrier doping by hydrogen in the spin-orbit coupled Mott insulator Sr₂IrO₄

Y. Yamashita,¹ G. Lim,¹ T. Maruyama,² A. Chikamatsu,² T. Hasegawa,² H. Ogino[ⓧ],³ T. Ozawa,⁴ M. Wilde,⁴ K. Fukutani,⁴ T. Terashima,⁵ M. Ochi,⁶ K. Kuroki,⁶ H. Kitagawa[ⓧ],¹ and M. Maesato[ⓧ],^{1,*}

¹*Division of Chemistry, Graduate School of Science, Kyoto University, Kitashirakawa Oiwake-cho, Sakyo-ku, Kyoto 606-8502, Japan*

²*Department of Chemistry, The University of Tokyo, 7-3-1 Hongo, Bunkyo-ku, Tokyo 113-0033, Japan*

³*National Institute of Advanced Industrial Science and Technology (AIST), 1-1-1 Umezono, Tsukuba, Ibaraki 305-8568, Japan*

⁴*Institute of Industrial Science, The University of Tokyo, 4-6-1 Komaba, Meguro-ku, Tokyo 153-8505, Japan*

⁵*Department of Physics, Graduate School of Science, Kyoto University, Kitashirakawa Oiwake-cho, Sakyo-ku, Kyoto 606-8502, Japan*

⁶*Department of Physics, Osaka University, Toyonaka, Osaka 560-0043, Japan*



(Received 3 May 2021; revised 16 June 2021; accepted 12 July 2021; published 27 July 2021)

Highly efficient carrier doping into the spin-orbit coupled Mott insulator Sr₂IrO₄ is achieved by low-energy hydrogen ion beam irradiation at low temperature. We demonstrate that heavy doping of hydrogen into a Sr₂IrO₄ epitaxial thin film induces a large increase in conductivity by band-filling control via electron doping, which is confirmed by Hall effect measurements. The introduction of a large amount of hydrogen and its distribution along the depth direction are clarified by nuclear reaction analysis. The doped interstitial and substitutional hydrogens act as electron donors with minimum perturbation to the lattice, as evidenced by crystal structural analysis and first-principles calculations of the defect formation energy for doped hydrogen. The hydrogen-doping method offers a strategy toward realization of novel quantum phases in strongly correlated spin-orbit entangled systems.

DOI: [10.1103/PhysRevB.104.L041111](https://doi.org/10.1103/PhysRevB.104.L041111)

The investigation of emergent quantum phases in strongly correlated systems with spin-orbit coupling is one of the central issues in modern condensed matter physics [1]. Recently, iridates have attracted much attention because the strength of spin-orbit coupling is comparable to those of crystal field splitting and on-site Coulomb interaction, giving rise to exotic electronic states such as a quantum spin liquid, a topological Mott insulator, a Weyl semimetal, and an electronic nematic (anapole) state [2–6]. The layered perovskite oxide Sr₂IrO₄ is of particular interest because it is the first example of a spin-orbit coupled Mott insulator [7,8]. The *t_{2g}* states with five valence electrons are split into a $J_{\text{eff}} = 1/2$ doublet and a $J_{\text{eff}} = 3/2$ quartet by spin-orbit coupling, leaving a half-filled $J_{\text{eff}} = 1/2$ band. The moderate on-site Coulomb repulsion induces a Mott gap and, therefore, the spin-orbit coupled $J_{\text{eff}} = 1/2$ Mott insulating state [7–10] with a canted antiferromagnetic ground state ($T_N = 240$ K) [11].

Because of the similarity with cuprates, carrier-doped Sr₂IrO₄ has been considered as an attractive candidate for a novel high-temperature superconductor [12–14]. The unconventional superconductivity has been predicted in doped Sr₂IrO₄ by theoretical studies [15–19], and the observations of Fermi arcs, pseudogaps [13,14,20], and a *d*-wave gap behavior [21] were reported in electron-doped Sr₂IrO₄. Even though a number of experimental investigations on carrier doping via chemical modification have been performed [22–26], the distinct signature of superconductivity has not been observed experimentally. Chemical substitution may involve structural modification of the host material, which can

result in unintentional alterations of other parameters besides the band filling. For instance, the electron doping through La substitution and oxygen depletion in Sr₂IrO₄ results in metallic behavior, but the accompanied structural distortion such as rotation of IrO₆ octahedra induces a change in the bandwidth [22,25,26]. Furthermore, solubility usually limits band-filling control of solids over a wide range.

To address these problems, we focused on a hydrogen ion beam irradiation method for carrier doping [27]. Hydrogen can enter into solids with minimum perturbation to the lattice because it has the smallest size among elements. The moderate electronegativity allows it to interact with many elements and electron systems. Moreover, a large amount of hydrogen can be introduced into solids by suppressing desorption at low temperature. Therefore the low-temperature hydrogen ion beam irradiation has a large potential to dramatically change the physical properties of materials [27–29].

In this Research Letter, we report highly efficient electron doping via hydrogen ion beam irradiation into Sr₂IrO₄ thin films with moderate perturbation of the host structure and, therefore, the bandwidth. First-principles calculations predict electron doping by interstitial and substitutional hydrogens, in good agreement with our experiments.

Epitaxial Sr₂IrO₄ thin films were fabricated on (LaAlO₃)_{0.3}(SrAl_{0.5}Ta_{0.5}O₃)_{0.7} (LSAT) (001) substrates using pulsed laser deposition (PLD). The LSAT and SrTiO₃ substrates have nearly the same in-plane lattice constant as Sr₂IrO₄ [30], but our previous experiments indicated that SrTiO₃ shows metallic conduction after hydrogen doping [28]. Therefore we chose the LSAT substrate, which remains insulating even after hydrogen doping. A KrF pulsed excimer laser was used for the deposition with a fluence of 1.5 J/cm²

*maesato@kuchem.kyoto-u.ac.jp

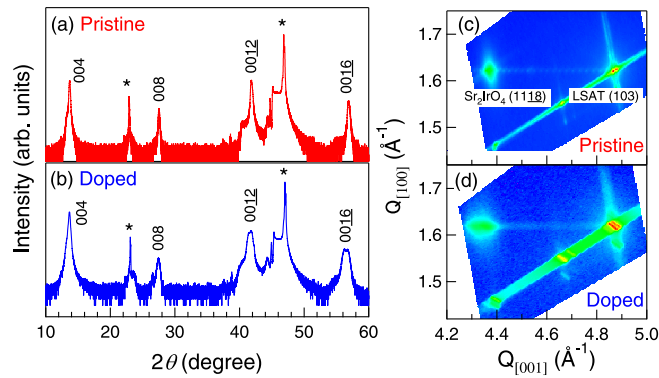


FIG. 1. X-ray diffraction 2θ - θ scan of the Sr_2IrO_4 thin film before (a) and after (b) hydrogen ion beam irradiation. The diffraction was measured at room temperature. The asterisks denote the $(00n)$ reflections from the LSAT substrate. (c) and (d) Reciprocal space mapping around the $(11\bar{1}8)$ reflection of the Sr_2IrO_4 and the (103) reflection of the LSAT substrate.

and a repetition rate of 1 Hz. The depositions were performed at a substrate temperature of 800°C and an oxygen partial pressure of 1 mTorr. Figure 1(a) shows the 2θ - θ x-ray diffraction (XRD) pattern of the pristine Sr_2IrO_4 thin film. The observed $(004n)$ diffraction peaks indicate the epitaxial growth of a highly c -axis-orientated Sr_2IrO_4 film. The calculated c -axis lattice constant, $c = 25.88(1) \text{ \AA}$, is in good agreement with the previous report [31]. To further investigate the structure, we performed x-ray reciprocal space mapping (RSM) around the Sr_2IrO_4 $(11\bar{1}8)$ and the LSAT (103) reflections, as shown in Fig. 1(c). The a -axis lattice constant of the thin film (substrate) calculated from the position of spots is $a = 5.47(2)[3.87(1)] \text{ \AA}$, indicating the coherent growth [$\sqrt{2}a(\text{LSAT}) = a(\text{Sr}_2\text{IrO}_4)$] of the single-crystalline film.

Hydrogen ions (H_2^+) were implanted several times into the Sr_2IrO_4 film at 100 K with an acceleration voltage of 2.5 kV. *In situ* transport measurements were performed using a van der Pauw method, and the results are shown in Figs. 2(a) and 2(b). We note that the resistivity is simply calculated from the thickness of the film. The pristine Sr_2IrO_4 thin film showed insulating behavior with a room-temperature resistivity of about 0.1 \Omega cm . Figure 2(b) displays the irradiation dose dependence of the resistivity at 100 K. Upon implanting hydrogen, the thin film shows a strong decrease in resistivity. The resistivity is almost saturated after high doses, where a decrease by three orders of magnitude is observed at 100 K. The total irradiation dose calculated from the integrated current incident onto the sample is $2.5 \times 10^{16} \text{ H}_2 \text{ ions/cm}^2$. The temperature dependence of the resistivity below 100 K was measured after each irradiation step as shown in Fig. 2(a). Although the resistivity below 100 K was reversible, the resistivity further decreased irreversibly when the sample was heated to room temperature after the final irradiation and cooled again. This irreversible behavior is presumably attributed to an increase in electrically active hydrogens and healing or migration of irradiation defects at temperatures above 100 K, as we shall see below.

Figures 1(b) and 1(d) show the 2θ - θ XRD pattern and the RSM of the hydrogen-doped Sr_2IrO_4 thin film, respectively.

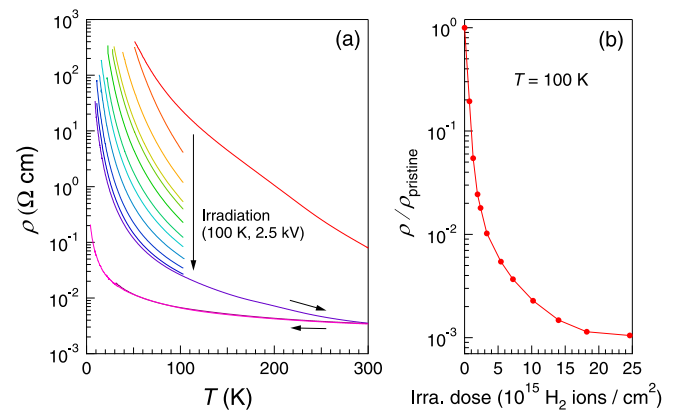


FIG. 2. (a) Temperature dependence of resistivity of pristine (top) and hydrogen-doped Sr_2IrO_4 thin films, in which hydrogen with an acceleration voltage of 2.5 kV was implanted in incremental doses at 100 K. The resistivity showed reversible temperature dependences below 100 K after the irradiations. A subsequent heating to 300 K after the final irradiation induced irreversible change in resistivity. (b) Dose dependence of resistivity under the hydrogen ion beam irradiation (Irra.) with an acceleration voltage of 2.5 kV at 100 K.

In the XRD pattern, although the doped sample exhibits the same diffraction peaks as the pristine one, we observed additional peaks shifting towards a lower angle for each $(004n)$ diffraction. The c -axis lattice constant is calculated as $c = 25.91(1)$ and $26.14(3) \text{ \AA}$ for the original and additional peaks, respectively. The change in the c -axis lattice constant is confirmed also by the RSM [Fig. 1(d)]. The 1% lattice expansion is attributable to the introduction of interstitial hydrogens, most probably near the apical oxygen. Hydrogens may reside in multiple locations to effectively spread the strain more uniformly than a localized distortion on a single sublattice.

In our experiments, the hydrogen ion beam irradiated the entire surface of the sample in normal incidence due to raster scanning, so that we believe that the hydrogen ions are implanted homogeneously in the surface plane. However, there should be a distribution of hydrogen along the depth direction because of the limited penetration depth of the implanted hydrogen ions. Therefore the above structural data indicate that only the near-surface region is lattice expanded due to the hydrogen introduction, while the deep nondoped region is not distorted. In previous reports on fluorinated Sr_2IrO_4 , fluorine ion layers were inserted between the IrO_4 layers, and the oxygens were partially replaced by fluorine, which resulted in large (40%) expansion of the c -axis lattice constant [32,33]. In comparison, the very modest change in the c -axis lattice constant safely excludes the possibility that intercalated hydrogen layers exist in the hydrogen-doped Sr_2IrO_4 . On the other hand, the in-plane a -axis lattice constant hardly changed [$a = 5.47(2) \text{ \AA}$] in the hydrogen-doped Sr_2IrO_4 as confirmed by RSM [Fig. 1(d)]. This suggests that the effect of the implanted hydrogen on the bandwidth via a possible change in the Ir-O-Ir bond angle is negligible.

We analyzed the resistivity data using a $\ln\rho$ - $T^{-1/4}$ plot in order to further examine the transport properties, as shown in Fig. S1 (see the Supplemental Material [34]). The pristine

sample followed the three-dimensional (3D) Mott variable range hopping (VRH) model below 100 K, which is consistent with previous reports [35]. The Mott VRH model is described as

$$\rho = \rho_0 \exp(T_0/T)^{1/4},$$

where ρ_0 and T_0 are constants [36]. For the VRH model to be valid, the mean hopping distance \bar{R}_M must be larger than the localization length a , which is given by $\frac{\bar{R}_M}{a} > 1$ [37]. The ratio is larger than 1 for both the pristine and doped samples; hence the requirement is satisfied. In the VRH model, the constant T_0 is related to the density of states at Fermi level $N(E_F)$ and the localization length a as

$$T_0 = \frac{18}{k_B a^3 N(E_F)}.$$

Assuming the localization length of 2 Å, to the first approximation, $N(E_F)$ for the doped and nondoped samples was calculated and is listed in Table S1 (see the Supplemental Material [34]). The $N(E_F)$ decreases once, upon the first hydrogen irradiation, but turns to increasing with increasing dose. The increase in $N(E_F)$ indicates the gradual increase in in-gap states due to doped (interstitial) hydrogens. The initial decrease may be in part attributed to substitutional hydrogens because the oxygen vacancies are considered to be filled preferentially with hydrogen as discussed later. It is noteworthy that $N(E_F)$ abruptly increased after the irreversible change in resistivity induced by the thermal excursion to 300 K. This behavior suggests that the amount of electronically active hydrogens increases with increasing temperature above 100 K.

After the hydrogen irradiation experiments in Fig. 2, *ex situ* Hall effect measurements for the film with the largest applied hydrogen dose were performed using a Physical Property Measurement System (PPMS, Quantum Design). The temperature dependences of carrier density and mobility calculated from the Hall effect measurements are shown in Figs. 3(a) and 3(b), respectively. Although a previous study reported *p*-type conduction in bulk Sr_2IrO_4 [38], the Hall coefficient for our pristine Sr_2IrO_4 thin film is negative. This probably originates from oxygen defects generated during the fabrication process [39]. The hydrogen-doped film exhibits *n*-type conduction with a drastic increase in carrier density. In addition, the carrier density is nearly temperature independent down to 200 K after the irradiation, indicating that the transport properties of the doped sample closely resemble those of degenerate semiconductors. Therefore we confirmed that highly efficient electron doping into Sr_2IrO_4 is achieved by the hydrogen ion beam irradiation. Figure 3(b) displays the carrier mobility for the pristine and hydrogen-doped Sr_2IrO_4 thin films, indicating nearly the same value and temperature dependence. The carrier mobility depends on scattering factors, such as phonons and impurities. Normally in doped semiconductors, the carrier mobility decreases with increasing doping amount at high carrier concentration because dopants act as a scattering center. The observed robustness of the mobility against hydrogen doping suggests that the contribution of impurity scattering to transport properties is not significant at least above 200 K. Since the lattice deformation induced by hydrogen injection is small, the effect on the lattice vibrational modes is also expected to be small. This may rationalize the observation

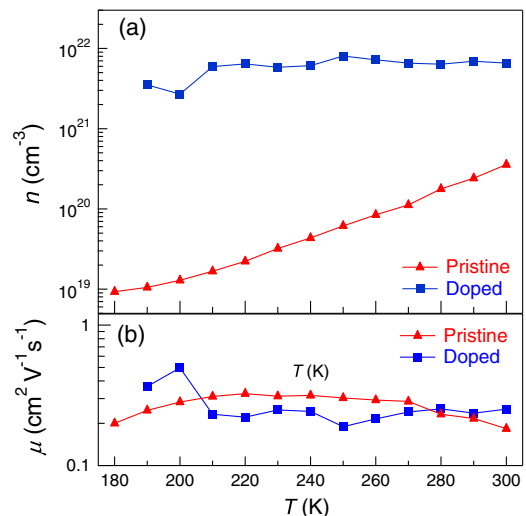


FIG. 3. (a) Carrier density and (b) mobility of the pristine (triangles) and hydrogen-doped (squares) Sr_2IrO_4 thin film obtained via *ex situ* Hall effect measurements. The magnetic field was applied along the *c* axis. The total hydrogen dose of $2.5 \times 10^{16} \text{H}_2$ ions/cm² was applied to the hydrogen-dosed Sr_2IrO_4 thin film as shown in Fig. 2.

that hydrogen doping does not seem to influence the carrier mobility to a large extent.

The distribution of hydrogen in the Sr_2IrO_4 thin film was examined by nuclear reaction analysis (NRA) via the $^1\text{H}(^{15}\text{N}, \alpha\gamma)^{12}\text{C}$ reaction in the Micro Analysis Laboratory, Tandem Accelerator (MALT), at the University of Tokyo [40,41]. The resonance width of the $^1\text{H}(^{15}\text{N}, \alpha\gamma)^{12}\text{C}$ reaction is sufficiently narrow, allowing for high-resolution depth profiling of hydrogen. In this experiment, a pristine Sr_2IrO_4 thin film was irradiated by hydrogen ions with an acceleration voltage of 2.5 kV at 100 K until the resistivity reached saturation. Figure 4 shows the depth profile of the hydrogen concentration, which indicates that the average penetration depth of implanted hydrogen is about 17 nm and that a large amount of hydrogen is actually introduced inside the Sr_2IrO_4 thin film. The sheet density of hydrogen ions calculated by integrating the depth profile is $4.8 \times 10^{16} \text{H atoms/cm}^2$, which is nearly identical to the applied saturation dose. The

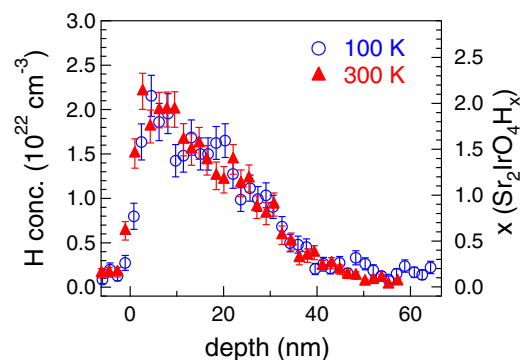


FIG. 4. Depth profile of hydrogen in the hydrogen-doped Sr_2IrO_4 thin film. The hydrogen was implanted with an acceleration voltage of 2.5 kV at 100 K until the resistivity reached saturation. conc., concentration.

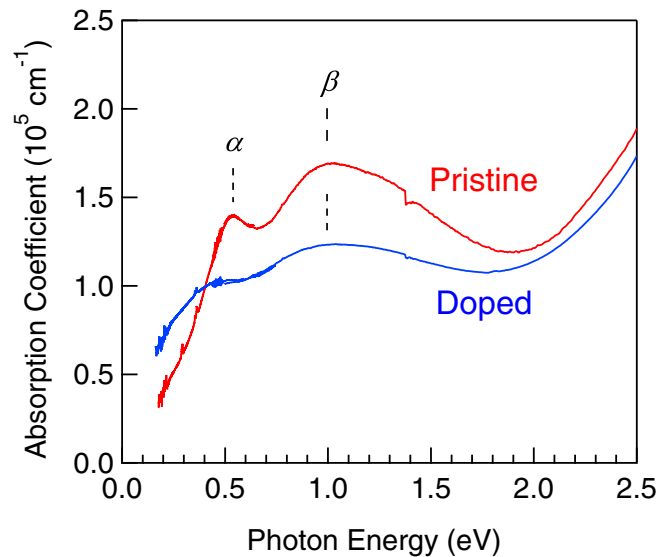


FIG. 5. Absorption coefficient spectra of the pristine and hydrogen-doped Sr_2IrO_4 thin films.

maximum hydrogen penetration depth is around 35 nm, which is smaller than the film thickness (~ 50 nm). Thus the deeper bulk region remains nondoped, in agreement with the results of XRD and RSM of the doped sample [Figs. 1(b) and 1(d)]. To examine the possibility of thermal diffusion and desorption of hydrogen, we investigated the temperature dependence of the hydrogen distribution. As seen in Fig. 4, the hydrogen profiles are almost identical at 100 and 300 K. Therefore, in this temperature region, long-range thermal diffusion and desorption of hydrogen are negligible.

Figure 5 shows the optical absorption coefficient spectra for the pristine and hydrogen-doped Sr_2IrO_4 thin film in the range of 0.2–2.5 eV. For the pristine sample, there are two absorption bands at 0.5 eV (α band) and 1.0 eV (β band) characteristic of Sr_2IrO_4 . The α peak is interpreted as the transition from the lower Hubbard band (LHB) to the upper Hubbard band (UHB) of the $J_{\text{eff}} = 1/2$ state, and the β peak is interpreted as the transition from the $J_{\text{eff}} = 3/2$ state to the UHB of the $J_{\text{eff}} = 1/2$ state. The $J_{\text{eff}} = 1/2$ model is based on an ideal cubic symmetry, and a deviation from cubic IrO_6 octahedra induces mixing between the $J_{\text{eff}} = 1/2$ and $J_{\text{eff}} =$

$3/2$ states. The previous fluorine-doping study reported that a large modulation of electronic states induced by fluorine insertion or substitution resulted in a blue shift of the β band because of the large difference in the electronegativity between oxygen and fluorine [32]. In sharp contrast, the position of the β band does not change in the hydrogen-doped Sr_2IrO_4 , indicating small perturbation to the lattice and therefore the J_{eff} states themselves. This suggests that the majority of doped hydrogens occupies interstitial sites near the apical oxygen. In addition, a low-energy excitation appears after the doping in good agreement with the increase in dc conductivity. The low-energy excitation indicates a spectral weight transfer from the Mott gap to the inner-gap regions for the doped sample, which is often observed in doped Mott insulators [42,43].

We performed a first-principles evaluation of the defect formation energy of the doped hydrogen in the way described in the Supplemental Material [34]. The calculated defect formation energies are -0.3 eV for H^- replacing the equatorial O^{2-} [Fig. 6(a)], $+0.3$ eV for interstitial H^+ neighboring the apical oxygen [Fig. 6(b)], and $+0.5$ eV for interstitial H^+ placed in the IrO_2 plane [Fig. 6(c)], when the Fermi level is located at the conduction band bottom. Note that a negative formation energy means that the defect is stable. Considering possible calculation errors originating from, e.g., a finite size of the supercell and theoretical difficulty to accurately treat the spin-orbit coupled Mott insulator, the precise determination of the defect formation energy is very challenging. Nevertheless, our calculation result of negative or relatively small defect formation energies suggests that the electron doping by hydrogen can take place in Sr_2IrO_4 . The interstitial hydrogen relatively favors the position near the apical oxygen, which is consistent with our experimental observation that the c -axis length is elongated while the a -axis length hardly changes by hydrogen doping. Also, considering that the pristine sample possesses a few oxygen defects, our simulation suggests that hydrogen possibly fills these vacancies.

We need to consider the potential for irradiation-induced damage to sample since the diffraction peaks of Sr_2IrO_4 were broadened after hydrogen irradiation. The annealing and/or migration of irradiation-induced defects may be one of the origins of irreversible change in resistivity at temperatures above 100 K because a reduction in the defect concentration is expected to reduce the resistivity. The irradiation defects may trap metastable hydrogen that can be electrically inert

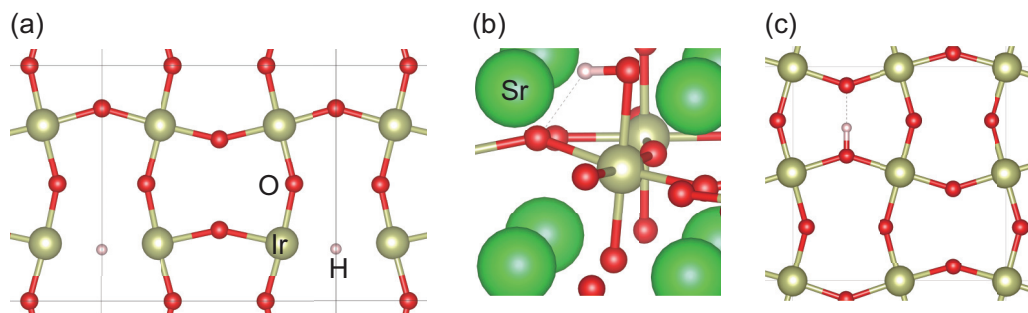


FIG. 6. Optimized crystal structures in first-principles calculations of Sr_2IrO_4 with several types of defects: (a) hydrogen replacing the equatorial oxygen, (b) interstitial hydrogen near the apical oxygen, and (c) interstitial hydrogen in the IrO_2 plane. The lines show the periodic cell in the calculation. These pictures were drawn using VESTA software [44].

just after implantation. The healing and/or migration of the defects could be associated with migration of hydrogens. Although we did not observe any change in the distribution of hydrogen up to 300 K by NRA, a local displacement of atoms may occur by heating to 300 K. Hydrogens that escaped from metastable trapping sites are considered to act as electron donors at elevated temperature, which can account for a large increase in the density of states.

We also note that the hydrogen concentration is not homogeneous along the depth direction. However, this can be improved by the use of thinner films or multiple irradiation steps with various acceleration energies because the average penetration depth of hydrogen depends on the acceleration energy. The appropriate choice of irradiation temperature and acceleration energy may improve the efficiency of carrier doping and homogeneity.

In summary, we investigated the effect of hydrogen doping on the conductivity of epitaxial Sr_2IrO_4 thin films utilizing low-temperature hydrogen ion beam irradiation. The *in situ* transport measurements revealed a large decrease in resistivity upon hydrogen doping and irreversible further decrease in resistivity by thermal treatment. The introduction of a large amount of hydrogen and its distribution along the depth direction were clarified by NRA. Hydrogen acts as a donor because

the hydrogen-doped Sr_2IrO_4 shows *n*-type conduction, which is in good agreement with the first-principles calculation of the defect formation energy for doped hydrogen. The absorption spectra, XRD, and RSM indicated that the doped hydrogens occupy interstitial or substitutional sites in Sr_2IrO_4 with minimum perturbation to the lattice and generate an in-gap state. Therefore low-temperature hydrogen ion beam irradiation is a powerful method for controlling physical properties of highly correlated iridates and exploring exotic phases such as a superconducting phase purely due to the band-filling effect.

We are grateful to H. Matsuzaki at the University of Tokyo for assistance in the MALT accelerator operation. This work was supported by JSPS KAKENHI (Grants No. JP19H05052, No. 20H02709, No. JP19H05058, JP18H05518, and No. JP20H05623). Parts of the numerical calculations were performed using the large-scale computer systems provided by the following institutions: the supercomputer center of the Institute for Solid State Physics, The University of Tokyo; the Information Technology Center, The University of Tokyo; and the Cybermedia Center, Osaka University. Computational resources from the Cybermedia Center were provided through the HPCI System Research Project (Project ID hp200007).

-
- [1] W. Witczak-Krempa, G. Chen, Y. B. Kim, and L. Balents, Correlated quantum phenomena in the strong spin-orbit regime, *Annu. Rev. Condens. Matter Phys.* **5**, 57 (2014).
- [2] K. Kitagawa, T. Takayama, Y. Matsumoto, A. Kato, R. Takano, Y. Kishimoto, S. Bette, R. Dinnebier, G. Jackeli, and H. Takagi, A spin-orbital-entangled quantum liquid on a honeycomb lattice, *Nature (London)* **554**, 341 (2018).
- [3] D. Pesin and L. Balents, Mott physics and band topology in materials with strong spin-orbit interaction, *Nat. Phys.* **6**, 376 (2010).
- [4] X. Wan, A. M. Turner, A. Vishwanath, and S. Y. Savrasov, Topological semimetal and Fermi-arc surface states in the electronic structure of pyrochlore iridates, *Phys. Rev. B* **83**, 205101 (2011).
- [5] K. Ueda, R. Kaneko, H. Ishizuka, J. Fujioka, N. Nagaosa, and Y. Tokura, Spontaneous Hall effect in the Weyl semimetal candidate of all-in all-out pyrochlore iridate, *Nat. Commun.* **9**, 3032 (2018).
- [6] H. Murayama, K. Ishida, R. Kurihara, T. Ono, Y. Sato, Y. Kasahara, H. Watanabe, Y. Yanase, G. Cao, Y. Mizukami, T. Shibauchi, Y. Matsuda, and S. Kasahara, Bond Directional Anapole Order in a Spin-Orbit Coupled Mott Insulator $\text{Sr}_2(\text{Ir}_{1-x}\text{Rh}_x)\text{O}_4$, *Phys. Rev. X* **11**, 011021 (2021).
- [7] B. J. Kim, H. Jin, S. J. Moon, J.-Y. Kim, B.-G. Park, C. S. Leem, J. Yu, T. W. Noh, C. Kim, S.-J. Oh, J.-H. Park, V. Durairaj, G. Cao, and E. Rotenberg, Novel $J_{\text{eff}} = 1/2$ Mott State Induced by Relativistic Spin-Orbit Coupling in Sr_2IrO_4 , *Phys. Rev. Lett.* **101**, 076402 (2008).
- [8] B. J. Kim, H. Ohsumi, T. Komesu, S. Sakai, T. Morita, H. Takagi, and T. Arima, Phase-sensitive observation of a spin-orbital Mott state in Sr_2IrO_4 , *Science* **323**, 1329 (2009).
- [9] S. J. Moon, H. Jin, K. W. Kim, W. S. Choi, Y. S. Lee, J. Yu, G. Cao, A. Sumi, H. Funakubo, C. Bernhard, and T. W. Noh, Dimensionality-Controlled Insulator-Metal Transition and Correlated Metallic State in *5d* Transition Metal Oxides $\text{Sr}_{n+1}\text{Ir}_n\text{O}_{3n+1}$ ($n = 1, 2$, and ∞), *Phys. Rev. Lett.* **101**, 226402 (2008).
- [10] H. Zhang, K. Haule, and D. Vanderbilt, Effective $J = 1/2$ Insulating State in Ruddlesden-Popper Iridates: An LDA + DMFT Study, *Phys. Rev. Lett.* **111**, 246402 (2013).
- [11] G. Cao, J. Bolivar, S. McCall, J. E. Crow, and R. P. Guertin, Weak ferromagnetism, metal-to-nonmetal transition, and negative differential resistivity in single-crystal Sr_2IrO_4 , *Phys. Rev. B* **57**, R11039(R) (1998).
- [12] J. Kim, D. Casa, M. H. Upton, T. Gog, Y.-J. Kim, J. F. Mitchell, M. van Veenendaal, M. Daghofer, J. van den Brink, G. Khaliullin, and B. J. Kim, Magnetic Excitation Spectra of Sr_2IrO_4 Probed by Resonant Inelastic X-Ray Scattering: Establishing Links to Cuprate Superconductors, *Phys. Rev. Lett.* **108**, 177003 (2012).
- [13] Y. K. Kim, O. Krupin, J. D. Denlinger, A. Bostwick, E. Rotenberg, Q. Zhao, J. F. Mitchell, J. W. Allen, and B. J. Kim, Fermi arcs in a doped pseudospin-1/2 Heisenberg antiferromagnet, *Science* **345**, 187 (2014).
- [14] Y. J. Yan, M. Q. Ren, H. C. Xu, B. P. Xie, R. Tao, H. Y. Choi, N. Lee, Y. J. Choi, T. Zhang, and D. L. Feng, Electron-Doped Sr_2IrO_4 : An Analogue of Hole-Doped Cuprate Superconductors Demonstrated by Scanning Tunneling Microscopy, *Phys. Rev. X* **5**, 041018 (2015).
- [15] F. Wang and T. Senthil, Twisted Hubbard Model For Sr_2IrO_4 : Magnetism and Possible High Temperature Superconductivity, *Phys. Rev. Lett.* **106**, 136402 (2011).

- [16] H. Watanabe, T. Shirakawa, and S. Yunoki, Monte Carlo Study of an Unconventional Superconducting Phase in Iridium Oxide $J_{\text{eff}}=1/2$ Mott Insulators Induced by Carrier Doping, *Phys. Rev. Lett.* **110**, 027002 (2013).
- [17] Z. Y. Meng, Y. B. Kim, and H.-Y. Kee, Odd-Parity Triplet Superconducting Phase in Multiorbital Materials with a Strong Spin-Orbit Coupling: Application to Doped Sr_2IrO_4 , *Phys. Rev. Lett.* **113**, 177003 (2014).
- [18] Y. Yang, W.-S. Wang, J.-G. Liu, H. Chen, J.-H. Dai, and Q.-H. Wang, Superconductivity in doped Sr_2IrO_4 : A functional renormalization group study, *Phys. Rev. B* **89**, 094518 (2014).
- [19] S. Sumita, T. Nomoto, and Y. Yanase, Multipole Superconductivity in Nonsymmorphic Sr_2IrO_4 , *Phys. Rev. Lett.* **119**, 027001 (2017).
- [20] I. Battisti, K. M. Bastiaans, V. Fedoseev, A. De La Torre, N. Iliopoulos, A. Tamai, E. C. Hunter, R. S. Perry, J. Zaanen, F. Baumberger, and M. P. Allan, Universality of pseudogap and emergent order in lightly doped Mott insulators, *Nat. Phys.* **13**, 21 (2017).
- [21] Y. K. Kim, N. H. Sung, J. D. Denlinger, and B. J. Kim, Observation of a d -wave gap in electron-doped Sr_2IrO_4 , *Nat. Phys.* **12**, 37 (2016).
- [22] M. Ge, T. F. Qi, O. B. Korneta, D. E. De Long, P. Schlottmann, W. P. Crummett, and G. Cao, Lattice-driven magnetoresistivity and metal-insulator transition in single-layered iridates, *Phys. Rev. B* **84**, 100402(R) (2011).
- [23] X. Chen, T. Hogan, D. Walkup, W. Zhou, M. Pokharel, M. Yao, W. Tian, T. Z. Ward, Y. Zhao, D. Parshall, C. Opeil, J. W. Lynn, V. Madhavan, and S. D. Wilson, Influence of electron doping on the ground state of $(\text{Sr}_{1-x}\text{La}_x)_2\text{IrO}_4$, *Phys. Rev. B* **92**, 075125 (2015).
- [24] I. N. Bhatti, R. S. Dhaka, and A. K. Pramanik, Effect of Cu^{2+} substitution in spin-orbit coupled $\text{Sr}_2\text{Ir}_{1-x}\text{Cu}_x\text{O}_4$: Structure, magnetism, and electronic properties, *Phys. Rev. B* **96**, 144433 (2017).
- [25] H. Gretarsson, N. H. Sung, J. Porras, J. Bertinshaw, C. Dietl, J. A. N. Bruin, A. F. Bangura, Y. K. Kim, R. Dinnebier, J. Kim, A. Al-Zein, M. Moretti Sala, M. Krisch, M. Le Tacon, B. Keimer, and B. J. Kim, Persistent Paramagnons Deep in the Metallic Phase of $\text{Sr}_{2-x}\text{La}_x\text{IrO}_4$, *Phys. Rev. Lett.* **117**, 107001 (2016).
- [26] O. B. Korneta, T. Qi, S. Chikara, S. Parkin, L. E. De Long, P. Schlottmann, and G. Cao, Electron-doped $\text{Sr}_2\text{IrO}_{4-\delta}$ ($0 \leq \delta \leq 0.04$): Evolution of a disordered $J_{\text{eff}} = \frac{1}{2}$ Mott insulator into an exotic metallic state, *Phys. Rev. B* **82**, 115117 (2010).
- [27] R. Nakayama, N. Suzuki, M. Maesato, T. Nagaoka, M. Arita, and H. Kitagawa, A compact low-temperature hydrogen ion beam apparatus for *in situ* physical property measurements, *Rev. Sci. Instrum.* **88**, 123904 (2017).
- [28] R. Nakayama, M. Maesato, T. Yamamoto, H. Kageyama, T. Terashima, and H. Kitagawa, Heavy interstitial hydrogen doping into SrTiO_3 , *Chem. Commun. (Cambridge)* **54**, 12439 (2018).
- [29] G. Lim, M. Maesato, R. Nakayama, D.-W. Lim, and H. Kitagawa, Reversible resistance switching by excess hydrogen doping in rutile TiO_2 , *Appl. Phys. Express* **13**, 105502 (2020).
- [30] J. Nichols, J. Terzic, E. G. Bittle, O. B. Korneta, L. E. De Long, J. W. Brill, G. Cao, and S. S. A. Seo, Tuning electronic structure via epitaxial strain in Sr_2IrO_4 thin films, *Appl. Phys. Lett.* **102**, 141908 (2013).
- [31] A. Seo, P. P. Stavropoulos, H.-H. Kim, K. Fürsich, M. Souri, J. G. Connell, H. Gretarsson, M. Minola, H. Y. Kee, and B. Keimer, Compressive strain induced enhancement of exchange interaction and short-range magnetic order in Sr_2IrO_4 investigated by Raman spectroscopy, *Phys. Rev. B* **100**, 165106 (2019).
- [32] T. Maruyama, A. Chikamatsu, T. Katayama, K. Kuramochi, H. Ogino, M. Kitamura, K. Horiba, H. Kumigashira, and T. Hasegawa, Influence of fluorination on electronic states and electron transport properties of Sr_2IrO_4 thin films, *J. Mater. Chem. C* **8**, 8268 (2020).
- [33] K. Kuramochi, T. Shimano, T. Nishio, H. Okabe, A. Koda, K. Horigane, J. Akimitsu, and H. Ogino, Synthesis and physical properties of the new iridium oxyfluoride $\text{Sr}_2\text{Ir}(\text{O}, \text{F})_{6-\delta}$ using a topochemical reaction method, *Phys. Rev. Mater.* **4**, 013403 (2020).
- [34] See Supplemental Material at <http://link.aps.org/supplemental/10.1103/PhysRevB.104.L041111> for the analysis of conducting properties and details on theoretical calculations, which includes Refs. [45–57].
- [35] C. Lu, A. Quindeau, H. Deniz, D. Preziosi, D. Hesse, and M. Alexe, Crossover of conduction mechanism in Sr_2IrO_4 epitaxial thin films, *Appl. Phys. Lett.* **105**, 082407 (2014).
- [36] N. Mott, Conduction in glasses containing transition metal ions, *J. Non-Cryst. Solids* **1**, 1 (1968).
- [37] R. Rosenbaum, Crossover from Mott to Efros-Shklovskii variable-range-hopping conductivity in In_xO_y films, *Phys. Rev. B* **44**, 3599 (1991).
- [38] Y. Klein and I. Terasaki, Insight on the electronic state of Sr_2IrO_4 revealed by cationic substitutions, *J. Phys.: Condens. Matter* **20**, 295201 (2008).
- [39] C. Lu, S. Dong, A. Quindeau, D. Preziosi, N. Hu, and M. Alexe, Dual gate control of bulk transport and magnetism in the spin-orbit insulator Sr_2IrO_4 , *Phys. Rev. B* **91**, 104401 (2015).
- [40] K. Fukutani, Below-surface behavior of hydrogen studied by nuclear reaction analysis, *Curr. Opin. Solid State Mater. Sci.* **6**, 153 (2002).
- [41] M. Wilde and K. Fukutani, Hydrogen detection near surfaces and shallow interfaces with resonant nuclear reaction analysis, *Surf. Sci. Rep.* **69**, 196 (2014).
- [42] M. Imada, A. Fujimori, and Y. Tokura, Metal-insulator transitions, *Rev. Mod. Phys.* **70**, 1039 (1998).
- [43] Y. Taguchi, Y. Tokura, T. Arima, and F. Inaba, Change of electronic structures with carrier doping in the highly correlated electron system $\text{Y}_{1-x}\text{Ca}_x\text{TiO}_3$, *Phys. Rev. B* **48**, 511 (1993).
- [44] K. Momma and F. Izumi, *VESTA3* for three-dimensional visualization of crystal, volumetric and morphology data, *J. Appl. Crystallogr.* **44**, 1272 (2011).
- [45] J. P. Perdew, K. Burke, and M. Ernzerhof, Generalized Gradient Approximation Made Simple, *Phys. Rev. Lett.* **77**, 3865 (1996).
- [46] S. L. Dudarev, G. A. Botton, S. Y. Savrasov, C. J. Humphreys, and A. P. Sutton, Electron-energy-loss spectra and the structural stability of nickel oxide: An LSDA+U study, *Phys. Rev. B* **57**, 1505 (1998).
- [47] G. Kresse and D. Joubert, From ultrasoft pseudopotentials to the projector augmented-wave method, *Phys. Rev. B* **59**, 1758 (1999).
- [48] G. Kresse and J. Hafner, *Ab initio* molecular dynamics for liquid metals, *Phys. Rev. B* **47**, 558 (1993).

- [49] G. Kresse and J. Hafner, *Ab initio* molecular-dynamics simulation of the liquid-metal–amorphous-semiconductor transition in germanium, *Phys. Rev. B* **49**, 14251 (1994).
- [50] G. Kresse and J. Furthmüller, Efficiency of ab-initio total energy calculations for metals and semiconductors using a plane-wave basis set, *Comput. Mater. Sci.* **6**, 15 (1996).
- [51] G. Kresse and J. Furthmüller, Efficient iterative schemes for *ab initio* total-energy calculations using a plane-wave basis set, *Phys. Rev. B* **54**, 11169 (1996).
- [52] Q. Huang, J. Soubeyroux, O. Chmaissem, I. Sora, A. Santoro, R. Cava, J. Krajewski, and W. Peck, Neutron powder diffraction study of the crystal structures of Sr_2RuO_4 and Sr_2IrO_4 at room temperature and at 10 K, *J. Solid State Chem.* **112**, 355 (1994).
- [53] Q. Li, G. Cao, S. Okamoto, J. Yi, W. Lin, B. C. Sales, J. Yan, R. Arita, J. Kuneš, A. V. Kozhevnikov, A. G. Eguiluz, M. Imada, Z. Gai, M. Pan, and D. G. Mandrus, Atomically resolved spectroscopic study of Sr_2IrO_4 : Experiment and theory, *Sci. Rep.* **3**, 3073 (2013).
- [54] H.-P. Komsa, T. T. Rantala, and A. Pasquarello, Finite-size supercell correction schemes for charged defect calculations, *Phys. Rev. B* **86**, 045112 (2012).
- [55] S. B. Zhang and J. E. Northrup, Chemical Potential Dependence of Defect Formation Energies in GaAs: Application to Ga Self-Diffusion, *Phys. Rev. Lett.* **67**, 2339 (1991).
- [56] R. Ruruli and X. Cartoixa, Theory of defects in one-dimensional systems: Application to Al-catalyzed Si nanowires, *Nano Lett.* **9**, 975 (2009).
- [57] S. Lany and A. Zunger, Assessment of correction methods for the band-gap problem and for finite-size effects in supercell defect calculations: Case studies for ZnO and GaAs, *Phys. Rev. B* **78**, 235104 (2008).